# A Systematic Iterative Procedure for Determining Granulator Operating Parameters

**Ka Y. Fung and Ka M. Ng**
Dept. of Chemical Engineering, Hong Kong University of Science and Technology, Clear Water Bay, Hong Kong

**Susumu Nakajima**
Science and Technology Research Center, Mitsubishi Chemical Corporation, Aoba-ku, Yokohama 227-8502, Japan

**Christianto Wibowo**
ClearWaterBay Technology, Inc., Walnut, CA 91789

*DOI 10.1002/aic.10940*
*Published online August 1, 2006 in Wiley InterScience (www.interscience.wiley.com).*

*A systematic iterative procedure is presented for determining granulator operating parameters to produce granules with desired product attributes. These include mean granule size, size distribution, porosity, strength, and spatial distribution of the constituent components. After selecting the equipment and binder, a preliminary experiment is performed to determine base case results, which usually do not match the desired attributes. The final product is obtained using an iterative procedure with both analyses and experiments. The qualitative analysis identifies the operating parameters that can effect changes to the off-spec attribute. This is followed by a quantitative analysis—based on simple physically based mathematical models in the form of sensitivity analysis—that determines the parameter that has the greatest effect on the relevant attribute. Experiments with the modified formulation and operating conditions are conducted and the entire procedure is repeated until the desired product is obtained. A system with lactose and starch using hydroxypropyl cellulose as binder in an agitated fluidized bed granulator (Hosokawa Micron Agglomaster™) is used to illustrate this procedure.* © 2006 American Institute of Chemical Engineers *AIChE J,* 52: 3189–3202, 2006
*Keywords: wet granulation, powder processing, fluidized bed granulator, agglomeration, solids processes*

## Introduction

Granulation has been used extensively for a wide range of materials including minerals, agricultural products, pharmaceuticals, detergents, food products, and specialty chemicals. In the chemical industries, it has been estimated that 60% of products are manufactured as particulates and a further 20% use powders as ingredients.[1] Many of these are high value-added products. Pharmaceuticals, with global sales reaching US$491.8 billion in 2003,[2] are delivered primarily in solid form and granulation is used extensively in their manufacturing processes.

Despite its widespread use, significant advances in understanding the fundamentals of granulation were not achieved until the last two decades.[3] For example, the importance of binder viscosity on granulation was first recognized by Ennis et al.[4] in the early 1990s. The effect of spraying conditions (such as droplet size) and binder properties (such as viscosity and surface tension) on nucleation,[5,6] granule consolidation,[7,8] and granule coalescence[9] were identified even more recently. In

Correspondence concerning this article should be addressed to K. M. Ng at kekmng@ust.hk.

addition to qualitative understanding of granulation phenomena, models of granule consolidation,[10,11] granule coalescence,[12-14] and the overall granulation process[15-17] have been developed. These models often contain parameters whose values for a specific set of materials for granulation might not be readily available. Compounded by the idiosyncrasies of the design and operations of various granulators, a priori prediction of how to produce the desired granules in a systematic manner is difficult.

At present, considerable trial and error is required to obtain the granulator operating parameters that would produce granules with the desired attributes. Such tuning highly depends on the operator's experience with the materials being granulated. For this reason, the more sensitive parameters in a fluidized bed granulator have been identified using population balance modeling and experiments.[18] These include the bed bowl charge, binder spray rate, air flow rate, input air temperature, binder spray rate, and binder droplet diameter. The goal of this article is to develop an iterative procedure that builds on all the recent advances, to facilitate the trial and error effort of nonspecialists. Instead of predicting the actual granulation process, the qualitative understanding and quantitative models are used to guide experimental runs with the aim of minimizing time and effort to get to the target. The procedure is illustrated with three examples on the granulation of starch and lactose in an agitated fluidized bed granulator.

## The Iterative Procedure

First, a base case is obtained by performing a preliminary experiment using suitable equipment and binder. These base case results are expected to deviate from the specifications. Because various parameters simultaneously affect the granulation process, it is often tricky to determine which parameter should be adjusted to achieve the desired product attributes. Therefore, the strategy is to use qualitative analysis to screen all the parameters involved to identify the most promising set of parameters, and then to perform quantitative analysis to identify the most effective parameter from this set. Further experiments are conducted with the modified operating parameters and the entire procedure is repeated until a product with the desired attributes is obtained.

### *Development of base case*

*Identification of Desired Product Attributes.* The first step toward developing a base case is the identification of desired product attributes, including mean granule size and particle size distribution (PSD), porosity, tensile strength, shape, and content uniformity. These attributes determine the product quality of the granules and affect how they should be processed. For example, granule size and porosity determine the dissolution rate of granules. Smaller granules possess larger interparticle force, which may lead to bridge formation in the hopper of solids processing equipment such as a tableting machine. Uniform distribution of ingredients within granules (intragranular content uniformity) and among granules (intergranular content uniformity) are also important, given that nonuniform distribution of active pharmaceutical ingredients (APIs) may lead to uneven rate of release.

*Selection of Equipment and Binder.* Three types of granulation methods are used in pharmaceutical processing: wet granulation, dry granulation, and melt granulation.[19] Pressure is applied in dry granulation to bring the constituent and binder particles together, whereas binder solution is sprayed on the powder bed in wet granulation to effect cohesion. In melt granulation, the solid binder is melted to form bridges among particles. The selection of the granulation method is mainly based on material properties.[20] We focus on wet granulation in this article.

Various equipment types can be used for wet granulation. A suitable granulator can be selected using a feed and product size map along with some heuristics based on material properties.[21] For example, a high shear mixer granulator is most suitable for handling cohesive materials and produces dense granules, whereas a fluidized bed granulator is a better option for producing granules with lower density. Detailed descriptions of different granulators can be found elsewhere.[19,22-24]

Binders are added during granulation to increase the cohesiveness of powder to form granules upon particle–particle impact. Examples of commonly used binders in pharmaceutical applications and their properties can be found in the literature.[25] Guidelines for picking a suitable binder are also available. For example, starch and glucose would constitute suitable binders for producing soft and hard granules, respectively.[26]

*Preliminary Experiments.* With the selected equipment and binder, a preliminary experiment is performed. Operating conditions for the base case can be obtained from the literature or by following equipment manufacturer's suggestions. Common characterization methods for different product attributes are summarized in Table 1. PSD could be quantified using the coefficient of variation (*CV*):

$$CV = \frac{d_{84} - d_{16}}{2d_{50}} \tag{1}$$

where $d_{16}$, $d_{50}$, and $d_{84}$ are particle sizes corresponding to 16, 50, and 84% weight fractions on the cumulative PSD. These base case results will be compared with the desired product attributes to determine how the process conditions should be modified. For a fair comparison, the mixing time and the post-binder-addition (drying) time are the same for all experiments.

**Table 1. Characterization Methods for Different Product Attributes**

| Product Attributes | Principle/Techniques for Measurement |
|---|---|
| Granule size and PSD | Sieving (dry, wet, air-jet)<br>Light scattering |
| Granule porosity | |
| Pore volume | Gas adsorption (BET analysis) |
| True density | Pycnometer |
| Granule shape | Image analysis |
| Content uniformity | Time-of-Flight Secondary Ion Mass Spectrometry (ToF-SIMS) |

## Screening of Operating Parameters

In general, a product attribute $P_i$ can be described by the following equation:

**Table 2. Look-up Table for the Effect of Operating Parameters on Product Attributes**

| Operating Parameter $\alpha_j$, $\beta_j$ | Product Attribute $P_i$: Mean Granule Size, $a^{cr}$ | CV of Granule Size Distribution | Granule Porosity, $\varepsilon$ | Granule Strength, $\sigma_t$ | Granule Shape Factor | Granule Content Uniformity |
|---|---|---|---|---|---|---|
| Binder | | | | | | |
| Spreading coefficient of liquid over solid, $\lambda_{LS}$ | + | | − | + | | |
| Binder viscosity, $\mu$ | +[1] | + | +[1] | +[1] | | − |
| Binder surface tension, $\sigma$ | +[2] | | +[2] | +[2] | | |
| Binder volume, $V$ | + | | +/−[3] | +[4] | | |
| Binder flow rate, $\dot{V}$ | + | + | | | | − |
| Equipment | | | | | | |
| Degree of binder dispersion | | − | | | | + |
| Spray droplet size, $d_d$ | +[5] | | | | | |
| Spray droplet size distribution | | +[5] | | | | |
| Process intensity | − | | − | | + | |
| Others | | | | | | |
| Constituent particle size | + | | + | − | | |
| Constituent particle PSD | − | | − | + | | |
| Post-binder-addition time | + | | − | | | |

*Notes:*
1. Valid when viscous force is dominant.
2. Valid when capillary force is dominant.
3. +, valid when viscous force is dominant; −, valid when capillary or frictional force is dominant.
4. Valid except for systems dominated by frictional force, which has a maximum granule strength at 20–30% pore saturation.
5. Valid when fluidized bed granulator is used.

$$P_i = P_i(\boldsymbol{\alpha}, \boldsymbol{\beta}, \mathbf{q}) \tag{2}$$

where $\boldsymbol{\alpha}$ represents equipment parameters such as granulation operating conditions, $\boldsymbol{\beta}$ represents nonequipment parameters such as physical properties, and $\mathbf{q}$ includes all the intermediate variables necessary for relating the product attribute to the parameters. Both qualitative and quantitative analyses are used to screen the parameters.

### *Qualitative relationships between operating parameters and product attributes*

Table 2 identifies qualitative relationships between operating parameters $\boldsymbol{\alpha}$ and $\boldsymbol{\beta}$ and product attributes from literature. A positive sign indicates that an increase in the parameter would lead to an increase in the value of the product attribute, while a negative sign indicates the reverse. For any product attribute that needs to be changed to meet the specifications, all the relevant parameters that can effect such a change are identified first. In most cases, the list of relevant parameters could be shortened by eliminating parameters that are harder to change. For example, it is certainly harder to change binder surface tension than binder flow rate. These cause–effect relationships are governed by the forces among the particles, which in turn depend on the materials and the granulator operating conditions, as explained below.

Particles are held together inside granules by the force due to the liquid bridge and inter-particle frictional force. The former is made up of capillary pressure and viscous effect. The latter arises from the normal force generated at interparticle contacts and should be considered for fine particles held by a nonviscous binder. The capillary number ($Ca$)

$$Ca = \frac{\mu U}{\sigma} \tag{3}$$

compares the relative strength of viscous and capillary effects.[4] Here, $\mu$ is binder dynamic viscosity, $\sigma$ is binder surface tension, and $U$ is the relative velocity between particles, which could be related to the granule radius ($a$) and average shear rate inside the granulator ($\dot{\gamma}$):

$$U = a\dot{\gamma} \tag{4}$$

The capillary effect is dominant at low shear rates, whereas the viscous effect dominates at high shear rates, which is the case for most industrially relevant conditions, with $Ca > 10^{-4}$.[27]

For this reason, many of the controllable operating parameters in a granulation process are associated with the binder. For example, larger, stronger, and denser granules can be produced if the binder spreads and forms a film over the powder surface.[28] Such a condition can be approximated by the spreading coefficient ($\lambda_{LS}$):

$$\lambda_{LS} = \sigma(\cos\theta - 1) \tag{5}$$

where $\theta$ is the contact angle. The surface tension and contact angle of commonly used binders are available.[25] In addition, a stronger attractive force to hold constituent particles from breaking away is needed to produce larger granules. This can be achieved by increasing either binder viscosity or surface tension, depending on whether viscous or capillary effect is dominant, respectively. However, there is an optimum viscosity for granule growth. An excessively viscous binder cannot be squeezed out between granules and inhibits growth.[29] Larger granules can also be obtained by increasing binder volume and flow rate because this increases the amount of liquid sprayed onto the granules, making the granules more deformable and therefore more susceptible to coalescence and growth. Although increasing binder flow rate tends to increase mean

granule size, the net effect is more complicated because binder flow rate can also affect binder droplet size distribution.

Binder dispersion in turn affects the PSD of the granules. Granules with a wide PSD are obtained if the binder is not dispersed evenly, leading to preferential growth at different locations inside the granulator.[30] Various parameters can affect the degree of binder dispersion. For example, a low viscosity binder disperses much easier than a viscous one, and binder delivered by atomization spreads more evenly than binder delivered by pouring. The degree of binder dispersion can be represented by the dimensionless spray flux $\psi_a$ [5]

$$\psi_a = \frac{3\dot{V}}{2\dot{A}d_d} \tag{6}$$

where $\dot{V}$ is the binder volumetric spray rate, $\dot{A}$ is the flux of powder surface traversing through the spray zone, and $d_d$ is the droplet diameter. With the same droplet diameter, a lower value of $\psi_a$ represents better binder dispersion. For spraying inside a fluidized bed granulator, the droplet size also affects the mean granule size, as given by the correlation

$$a \propto d_d^n \tag{7}$$

where $n$ is a constant between 0 and 1. Therefore, a narrower PSD can be obtained by decreasing the binder spray rate and by controlling the nozzle position and the spray angle inside granulator, whereas larger granules can be obtained by increasing the droplet size.

Granule porosity and strength are both related to the PSD of the constituent particles as well as to each other. Granules of fine particles with a wide size distribution are generally stronger as a result of the higher density of interparticle contacts. A longer post-binder-addition time also compacts the granules, up to the minimum porosity. Also, the smaller pore size among particles lead to an increase in the capillary or viscous effect inside granules, which contributes to the granule strength. Because these granules are less deformable because of lower internal porosity, they tend to grow slowly and have a smaller final size. A more complicated picture exists on the effect of binder volume, which depends on the dominant force inside granules. When the viscous effect is dominant, increasing binder volume increases the binding force and granule strength, concomitantly reducing particle mobility and producing less compact granules. If frictional force is dominant, increasing liquid content at low saturation levels increases particle mobility to form a more compact granule, thus increasing granule strength. However, at higher saturation levels, the effect of binder lubrication becomes significant and increasing liquid content reduces frictional force and granule strength. The maximum strength occurs at 20–30% liquid saturation.[3]

Little is discussed in the literature on the effect of operating parameters on granule shape. It is known that granules are more spherical at higher impeller speed or fluidization velocity. At such high process intensity, smaller granules are produced as a consequence of more frequent breakage inside the granulator. The amount of consolidation also escalates, leading to denser granules. The ingredients are distributed more uniformly within and among granules if the binder is dispersed evenly inside the granulator. This provides uniform wetting over the powder surface, reducing the chances of preferential wetting over the hydrophilic particles.

### *Quantitative models relating operating parameters to product attributes*

After identifying a list of parameters that are likely to be effective in modifying a product attribute (Table 2), we need to quantify the relative impact of each parameter and to identify the required change in the parameter to achieve the desired product attribute. To this end, sensitivity coefficients, $S_{\alpha_j}^{P_i}$, will be obtained from the product attribute general model (Eq. 2) by the direct differentiation method.[31] It shows the dependency of $P_i$ on $\alpha_j$ or, equivalently, $\beta_j$, with or without the presence of a set of intermediate variables $\mathbf{q}$:

$$S_{\alpha_j}^{P_i} = \left[\frac{\partial P_i}{\partial \alpha_j}\right]_{\alpha_{j,0}} = \sum_k \left[\frac{\partial P_i}{\partial q_k}\frac{\partial q_k}{\partial \alpha_j}\right]_{\alpha_{j,0}} \tag{8}$$

In general, the parameters $\alpha_j$ can differ by orders of magnitude. For example, binder viscosity is usually in the order of $10^{-2}$ to $10^{-3}$ Pa·s, whereas binder flow rate is usually in the order of $10^{-7}$ to $10^{-8}$ m$^3$/s. To compare the effect of these parameters on an equal basis, a set of normalized sensitivity coefficients $\bar{S}_{\alpha_j}^{P_i}$ are used instead:

$$\bar{S}_{\alpha_j}^{P_i} = \left[\frac{\partial P_i}{\partial \alpha_j/\Delta\alpha_{j,\max}}\right]_{\alpha_{j,0}} = S_{\alpha_j}^{P_i}\Delta\alpha_{j,\max} \tag{9}$$

where $\Delta\alpha_{j,\max}$ is the maximum expected range of $\alpha_j$. The larger the absolute value of a normalized sensitivity coefficient, the more impact the corresponding parameter exerts on the product attribute.

After identifying the most effective parameter, the required change in the parameter to obtain the desired product attribute can be estimated using finite-difference approximation:

$$\Delta P_i = \sum_j \bar{S}_{\alpha_j}^{P_i}\frac{\Delta\alpha_j}{\Delta\alpha_{j,\max}} \tag{10}$$

Experiments are then performed with the new operating conditions. If the new experimental results do not match the estimations from this quantitative analysis, as will be demonstrated in the examples below, any uncertainties in Eq. 8 are removed using the experimental data. This will help improve the accuracy of the predictions in subsequent iterations.

Models describing mean granule size, PSD, granule porosity, and tensile strength are summarized in Table 3, which also shows the intermediate variables such as thickness of liquid layer $h$, dimensionless penetration time $\tau_p$, and granule porosity $\varepsilon$. If no established relations exist between $\mathbf{q}$ and either $P_i$ or $\alpha_j$, expressions for $\partial P_i/\partial q_k$ or $\partial q_k/\partial \alpha_j$ in the sensitivity coefficient obviously cannot be evaluated. In such cases, these terms are estimated through experiments. Table 4 gives order of magnitude estimates of some of these terms for typical granulation processes, which can be used as initial guesses in the absence of better information. For example, changes in binder layer

**Table 3. Models Used in Quantitative Analysis**

| Product Attributes ($P$) | Intermediate Variables ($q$) | Relationships | |
|---|---|---|---|
| Granule size, $a^{cr}$ | Thickness of liquid layer, $h$ | If $a^{cr}_{coal} < a^{cr}_{def}$, $a^{cr} = (1 - f_1)a^{cr}_{coal} + f_1 a^{cr}_{def}$ | (11) |
| | Critical Stokes' number for deformation, $\mathrm{St}^*_{def}$ | If $a^{cr}_{coal} > a^{cr}_{def}$, $a^{cr} = a^{cr}_{def}$ | (12) |
| | | where | |
| | | $a^{cr}_{def} = \left(\frac{2\tau_y \mathrm{St}^*_{def}}{\rho_p \dot{\gamma}^2}\right)^{0.5}$ | (13) |
| | | If capillary effect is dominant, | |
| | | $a^{cr}_{coal} = a^{cr}_{c,coal} = \left(\frac{3\sigma F_{c0} h\, \mathrm{St}^*_{c,coal}}{4\rho_p \dot{\gamma}^2}\right)^{0.25}$ | (14) |
| | | $\mathrm{St}^*_{c,coal} = 2\left(\frac{1}{e^2} - 1\right)\left(1 - \frac{h_a}{h}\right)$ | (15) |
| | | If viscous effect is dominant, | |
| | | $a^{cr}_{coal} = a^{cr}_{v,coal} = \left(\frac{9\mu\, \mathrm{St}^*_{v,coal}}{8\rho_p \dot{\gamma}}\right)^{0.5}$ | (16) |
| | | $\mathrm{St}^*_{v,coal} = \left(1 + \frac{1}{e}\right)\ln\left(\frac{h}{h_a}\right)$ | (17) |
| Granule PSD, CV | Dimensionless penetration time, $\tau_p$ | For operating conditions inside the nucleation or induction regime of the granule growth regime map: | |
| | Dimensionless spray flux, $\psi_a$ (Eq. 6) | $\tau_p = \frac{t_p}{t_c}$ | (18) |
| | | $t_p = 1.35\, \frac{V_d^{2/3}}{\varepsilon_b^2 R_{pore}} \frac{\mu}{\sigma \cos\theta}$ | (19) |
| Granule porosity, $\varepsilon$ | Thickness of liquid layer, $h$ | If capillary effect is dominant, | |
| | | $\frac{\varepsilon_{\min}}{(1 - \varepsilon_{\min})^3} = \frac{1}{K_\varepsilon}$ | (20) |
| | | $K_\varepsilon = \frac{32}{3} \frac{\rho_p g H_{\max}}{f(\mu)} \frac{a}{\phi(s)\sigma \cos\theta}$ | (21) |
| | | If viscous effect is dominant, | |
| | | $h = \frac{h_0}{2}[1 + \exp(-\mathrm{St}_{v,coal})]$ | (22) |
| | | $\mathrm{St}_{v,coal} = \frac{8\rho_p U a}{9\mu}$ | (23) |
| | | $\frac{d\varepsilon}{dh} = \frac{3(1 - \varepsilon)}{a + h}$ | (24) |
| Tensile strength, $\sigma_t$ | Granule porosity, $\varepsilon$ | $\sigma_t = sC \frac{1 - \varepsilon}{\varepsilon} \frac{\sigma \cos\theta}{2a}$ | (25) |

thickness and binder flow rate are typically in the order of $10^{-7}$ to $10^{-6}$ m and $10^{-8}$ m$^3$/s, respectively, leading to a value of $10^1$ to $10^2$ s/m$^2$ for $\partial h/\partial \dot{V}$. The models in Table 3 are briefly described below.

Granule size can be modeled by considering the two key mechanisms that determine the final granule size: coalescence and breakage. Larger granules form as a result of successful coalescence of smaller granules. Granules can also deform and break up into smaller pieces when they collide. Using critical values of the Stokes' number (St), which signifies the relative importance of rebound velocity in a collision compared to the capillary or viscous effect that holds the granule together, critical sizes for granule coalescence ($a^{cr}_{coal}$) and deformation ($a^{cr}_{def}$) can be obtained.[11] Collision of granules of sizes above $a^{cr}_{coal}$ does not lead to coalescence to form larger granules. Granules of sizes above $a^{cr}_{def}$ deform and break up into smaller granules when they collide.

Two outcomes are possible depending on the relative values

**Table 4. Order of Magnitude for Differential Terms $\partial P_i/\partial q_k$ or $\partial q_k/\partial \alpha_j$ Used in Sensitivity Analysis**

| | $P_i$ or $q_k$ | | |
|---|---|---|---|
| $q_k$ or $\alpha_j$ | Binder Layer Thickness, $h$ (m) | Critical Stokes' Number for Deformation, $\mathrm{St}^*_{def}$ | Coefficient of Variation, $CV$ |
| Binder viscosity, $\mu$ (Pa · s) | — | (+), $10^0$–$10^1$ | — |
| Binder flow rate, $\dot{V}$ (m$^3$/s) | (+), $10^1$–$10^2$ | (+), $10^5$–$10^6$ | — |
| Binder volume, $V$ (m$^3$) | (+), $10^{-3}$–$10^{-2}$ | (+), $10^1$–$10^3$ | — |
| Fluidized air velocity, $U$ (m/s) | (−), $10^{-6}$–$10^{-5}$ | (−), $10^{-1}$–$10^0$ | — |
| Dimensionless spray flux, $\psi_a$ | — | — | (+), $10^{-2}$–$10^0$ |
| Dimensionless penetration time, $\tau_p$ | — | — | (+), $10^{-2}$–$10^0$ |

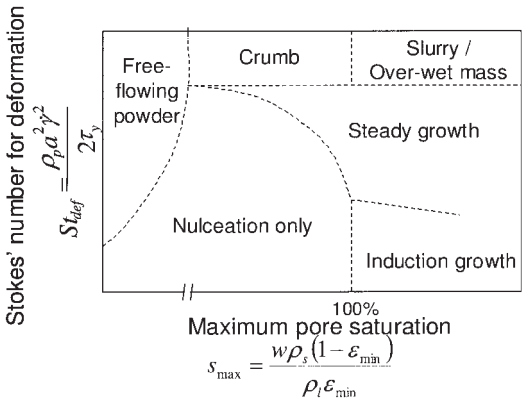


**Figure 1. Granule growth regime map (after Iveson et al.[9]).**

of these critical sizes. If $a_{coal}^{cr} < a_{def}^{cr}$, the granule size will stabilize at a size between $a_{coal}^{cr}$ and $a_{def}^{cr}$ for the reasons given below. Granules of size larger than $a_{def}^{cr}$ cannot exist as a result of breakup. For granules of size smaller than $a_{coal}^{cr}$, they grow larger as a result of coalescence. In addition, small granules can grow by layering to produce granules that are larger than $a_{coal}^{cr}$. The parameter $f_1$ ($0 \leq f_1 \leq 1$) in Eq. 11 represents the importance of layering on granule growth; a larger $f_1$ implies more layering. Depending on the dominant force inside granules, the coalescence critical size based on capillary effect ($a_{c,coal}^{cr}$) or viscous effect ($a_{v,coal}^{cr}$) is defined by Eqs. 14 and 16 in Table 3, respectively.[11] If $a_{coal}^{cr} > a_{def}^{cr}$, the granule size will stabilize at $a_{def}^{cr}$ as given in Eq. 12.[32] An expression relating $St_{def}^{*}$ to other operating parameters is not available but it can be determined experimentally using a fluidized bed Couette device.[32] As a general guideline, experiments show that $St_{def}^{*}$ generally assumes an order of magnitude of unity.

Established relationships between PSD and operating parameters are available only if the operating conditions are located inside the nucleation or induction regime of the granule growth regime map (Figure 1), which identifies the growth behavior at different maximum pore saturation ($s_{max}$) and Stokes' number for deformation ($St_{def}$). In these regions, PSD is controlled by nuclei size distribution because the granules are not sufficiently deformable and the pores are not sufficiently saturated to produce a binder layer on the granule surface for coalescence.[9] Nucleation behavior depends on two intermediate variables: dimensionless spray flux ($\psi_a$) and dimensionless penetration time ($\tau_p$), as shown in the nucleation regime map in Figure 2.[6,33] A narrow nuclei size distribution is obtained if the operating conditions are located inside the drop-controlled regime where one drop produces one nucleus. Outside this regime, drop coalescence occurs, leading to a broader nuclei size distribution.

Granules gradually consolidate to a lower porosity if the collision force overcomes the resisting force inside the granules. When the capillary effect is dominant, minimum porosity ($\varepsilon_{min}$) can be expressed as a function of the dimensionless granule compaction rate ($K_\varepsilon$; Eq. 20).[10] When the viscous effect is dominant, a different model featuring interparticle gap distance as a measure of porosity is more suitable. The reduction in interparticle gap distance ($\Delta x$) increases with increasing Stokes' number for viscous effect ($St_{v,coal}$). By replacing $\Delta x$ in the equation by Ennis et al.[11] with $2(h_0 - h)$, Eq. 22 is obtained. Here, $h_0$ and $h$ are the thicknesses of liquid layer before and after consolidation, respectively. To obtain the sensitivity coefficient of $\varepsilon$ with respect to $\alpha_j$, the value of $d\varepsilon/dh$ is estimated by considering the consolidation of equal-size particles with initial porosity $\varepsilon_0$ (Eq. 24). Derivation of this equation is given in the Appendix.

Tensile strength is closely related to porosity; a more porous granule has a lower tensile strength. A model assuming capillary force being dominant (Eq. 25) has been used in a wide range of applications in the area of powder technology, including the design of hoppers and bins.[34]

## Examples

Three examples focusing on PSD (Example 1), granule porosity (Example 2), and uniformity of spatial distribution of an active ingredient (Example 3) are now discussed to illustrate the application of this approach in qualitatively screening the operating parameters and identifying the suitable changes for producing granules with the desired attributes. An agitated fluidized bed granulator (Model AGM-2-PJ; Hosokawa Micron Corporation) is used for all experiments. As shown in the schematic diagram in Figure 3, heated air enters at the bottom of the chamber. A distributor and a slit disk are used to distribute air evenly across the cross-sectional area. Inlet air and the tumbling action of the agitator blade provide fluidization of powders. The binder is atomized through the nozzle and sprayed onto the powders. Sufficiently small particles are carried by the fluidized air to the upper part of the chamber where they are trapped by filters. Compressed air passes intermittently through the filters to eject these small particles back to the chamber. Temperature indicators are available to measure product and exhaust temperature, and a temperature controller controls the fluidized air temperature at the inlet. Pressure indicators are also available to measure inlet, chamber, and exhaust pressures along the process, which could be adjusted using the forced and exhaust blowers. Correlation is provided to convert the pressure measured at the suction inlet air to fluidized air velocity. A humidity probe is also used to measure the humidity of the exhaust air. A pulse jet intermittently issues compressed air, allowing granulation and coating of submicron particles. For all experiments, the powder was mixed for about 10 and 15 min, before and after binder addition, respectively.

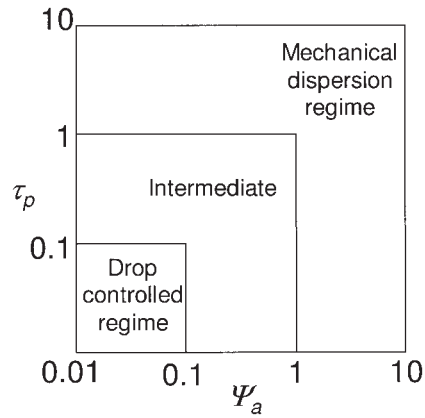


**Figure 2. Nucleation regime map (after Hapgood et al.[6]).**

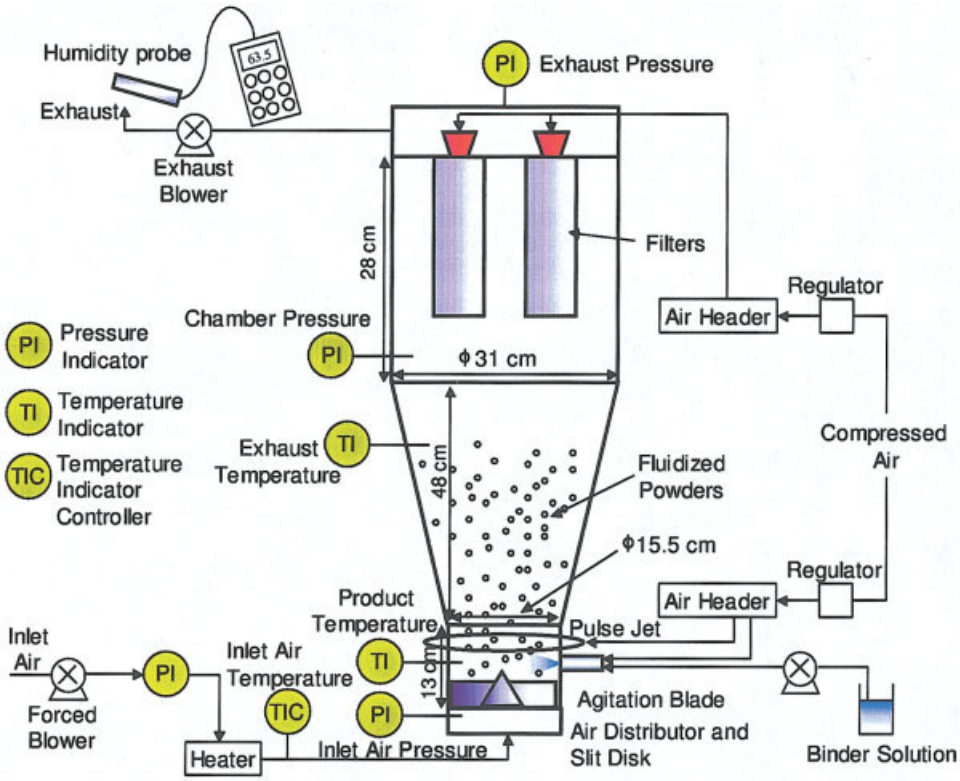


**Figure 3. Hosokawa Micron Agglomaster™.**

[Color figure can be viewed in the online issue, which is available at www.interscience.wiley.com]

### *Example 1*

The objective is to produce granules with a mean size of 80 $\mu$m and a CV of 0.85 from a mixture of starch and lactose using hydroxypropyl cellulose as binder. Preliminary operating conditions as suggested by Hosokawa Micron Corporation as well as other relevant input information for the base case are summarized in Table 5, where some of the estimated parameters were assumed based on typical values from various references.[11,32] The mean granule size measured with a laser diffraction particle size analyzer (Model LS13320; Beckman Coulter) was 50 $\mu$m. The corresponding particle size distribution, which had a CV of 0.73, is shown in Figure 4. A photomicrograph of typical granules for the base case is shown in Figure 5. The results of all experiments are summarized in Table 6.

Because the mean granule size in the base case was much smaller than the desired value, the formulation and operating conditions must be modified. First, the dominant force among particles was identified by calculating the capillary number using Eq. 3 with input values from Table 5. Given that $Ca = 0.1$, the viscous effect dominates. From the list of all parameters that can be used to increase the mean granule size (Table 2), we began by modifying parameters that were easier to change in practice: binder viscosity, flow rate, and volume. Changing other parameters such as constituent particle size and its distribution is not desirable because this requires pretreatment of the raw materials. Spray droplet size and its distribution are more difficult to adjust because they depend on the characteristics of the nozzle and the spraying conditions. Changing binder contact angle is also difficult because it might require the addition of a surfactant.

Sensitivity analysis of binder viscosity, flow rate, and volume on mean granule size was then carried out to quantify the relative effects of these parameters. Using the general model for product attribute (Eq. 2), the mean granule size can be expressed as

$$a^{cr} = a^{cr}(\mu, \dot{V}, V, h, \mathrm{St}^*_{def}) \tag{26}$$

Because $a^{cr}_{coal} < a^{cr}_{def}$ and the viscous effect dominates in the system, Eqs. 11, 13, 16, and 17 were used to constitute the granule size model, and the normalized sensitivity coefficients are expressed as

$$\begin{aligned}\bar{S}^{a^{cr}}_{\mu} &= \left[(1-f_1)\frac{\partial a^{cr}_{v,coal}}{\partial \mu} + f_1 \frac{\partial a^{cr}_{def}}{\partial\, \mathrm{St}^*_{def}} \frac{\partial\, \mathrm{St}^*_{def}}{\partial \mu}\right]_{\mu_0} \Delta\mu_{\max} \\ &= \left\{(1-f_1)\left[\frac{9}{32\rho_p \dot{\gamma}\mu_0}\left(1+\frac{1}{e}\right)\ln\frac{h_0}{h_a}\right]^{0.5} \right. \\ &\quad \left. + f_1\left(\frac{\tau_y}{2\rho_p\dot{\gamma}^2\mathrm{St}^*_{def}}\right)^{0.5}\frac{\partial\, \mathrm{St}^*_{def}}{\partial \mu}\right\}\Delta\mu_{\max}\end{aligned} \tag{27}$$

$$\bar{S}^{a^{cr}}_{V} = \left[(1-f_1)\frac{\partial a^{cr}_{v,coal}}{\partial h}\frac{\partial h}{\partial \dot{V}} + f_1 \frac{\partial a^{cr}_{def}}{\partial\, \mathrm{St}^*_{def}}\frac{\partial\, \mathrm{St}^*_{def}}{\partial \dot{V}}\right]_{\dot{V}_0} \Delta\dot{V}_{\max}$$

**Table 5. Operating Conditions and Physical Parameters for Example 1**

| | |
|---|---|
| Formulation and operating conditions | |
| Mass of lactose | 350 g |
| Mass of starch | 150 g |
| Binder spray position | Tangential spray |
| Binder volume, $V$ | 394 $cm^3$ |
| Binder concentration | 5 wt % |
| Binder viscosity, $\mu$ | 5 mPa · s |
| Binder flow rate, $\dot{V}$ | 11 g/min |
| Binder surface tension, $\sigma$ | 46 mN/m |
| Binder contact angle, $\theta$ | 34° |
| Pure liquid binder density | 1.24 g/mL |
| Fluidized air velocity, $U$ | 0.84 m/s |
| Fluidized air temperature | 60°C |
| Rotating disc speed | 300 rpm |
| Pulse jet | Off |
| Droplet diameter, $d_d$ | 26 $\mu$m |
| Post-binder-addition time | 15 min |
| Estimated parameters | |
| $h/h_a$ | 5 |
| Surface asperities, $h_a$ | 0.5 $\mu$m |
| Particle density, $\rho_p$ | 2000 kg/$m^3$ |
| Average shear rate inside granulator, $\dot{\gamma}$ | 9000 $s^{-1}$ |
| Coefficient of restitution, $e$ | 0.5 |
| Yield strength, $\tau_y$ | 3000 Pa |
| Critical value for Stokes' number for deformation, $St^*_{def}$ | 0.5 |
| $f_1$ | 0.8 |
| Powder flux, $\dot{A}$ | 0.021 $m^2$/s |
| Powder bed porosity, $\varepsilon_b$ | 0.097 |
| Pore radius, $R_{pore}$ | 0.36 $\mu$m |
| Circulation time, $t_c$ | 0.056 s |
| Maximum change of viscosity $\Delta\mu_{max}$ (Base case) | 30 mPa · s |
| Maximum change of viscosity $\Delta\mu_{max}$ (Run 2) | 15 mPa · s |
| Maximum change of binder flow rate $\Delta\dot{V}_{max}$ | $3 \times 10^{-7}$ $m^3$/s |
| Maximum change of binder volume $\Delta V_{max}$ | $2 \times 10^{-4}$ $m^3$ |
| $\frac{\partial h}{\partial \dot{V}}$ | 20 s/$m^2$ |
| $\frac{\partial h}{\partial V}$ | 0.015 $m^{-2}$ |
| $\frac{\partial\, St^*_{def}}{\partial \mu}$ | 2 (Pa · s)$^{-1}$ |
| $\frac{\partial\, St^*_{def}}{\partial \dot{V}}$ | $6 \times 10^5$ s/$m^3$ |
| $\frac{\partial\, St^*_{def}}{\partial V}$ | 100 $m^{-3}$ |
| $\frac{\partial CV}{\partial \psi_a}$ | 0.5 |
| $\frac{\partial CV}{\partial \tau_p}$ | 0.5 |

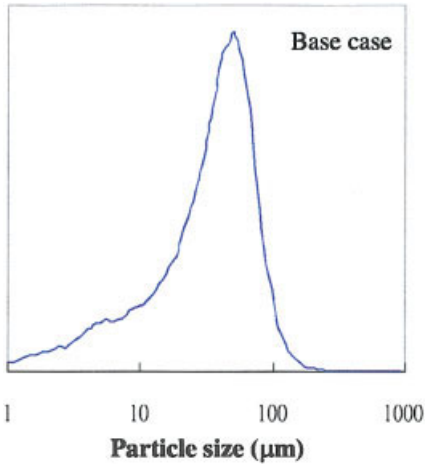


**Figure 4. Particle size distribution for base case in Example 1.**

[Color figure can be viewed in the online issue, which is available at www.interscience.wiley.com]

$$= \left\{ \frac{(1-f_1)}{h} \left[ \frac{9\mu_0}{32\rho_p \dot{\gamma}} \left(1+\frac{1}{e}\right) \right]^{0.5} \left( \ln \frac{h_0}{h_a} \right)^{-0.5} \frac{\partial h}{\partial \dot{V}} + f_1 \left( \frac{\tau_y}{2\rho_p \dot{\gamma}^2 St^*_{def}} \right)^{0.5} \frac{\partial\, St^*_{def}}{\partial \dot{V}} \right\} \Delta \dot{V}_{max} \quad (28)$$

$$\bar{S}^{a^{cr}}_V = \left[ (1-f_1) \frac{\partial a^{cr}_{v,coal}}{\partial h} \frac{\partial h}{\partial V} + f_1 \frac{\partial a^{cr}_{def}}{\partial\, St^*_{def}} \frac{\partial\, St^*_{def}}{\partial V} \right]_{V_0} \Delta V_{max}$$

$$= \left\{ \frac{(1-f_1)}{h} \left[ \frac{9\mu_0}{32\rho_p \dot{\gamma}} \left(1+\frac{1}{e}\right) \right]^{0.5} \left( \ln \frac{h_0}{h_a} \right)^{-0.5} \frac{\partial h}{\partial V} + f_1 \left( \frac{\tau_y}{2\rho_p \dot{\gamma}^2 St^*_{def}} \right)^{0.5} \frac{\partial\, St^*_{def}}{\partial V} \right\} \Delta V_{max} \quad (29)$$

Using input values from Table 5, $\bar{S}^{a^{cr}}_{\mu}$, $\bar{S}^{a^{cr}}_{\dot{V}}$, and $\bar{S}^{a^{cr}}_{V}$ were calculated to be $2.98 \times 10^{-5}$, $2.54 \times 10^{-5}$, and $5.07 \times 10^{-6}$

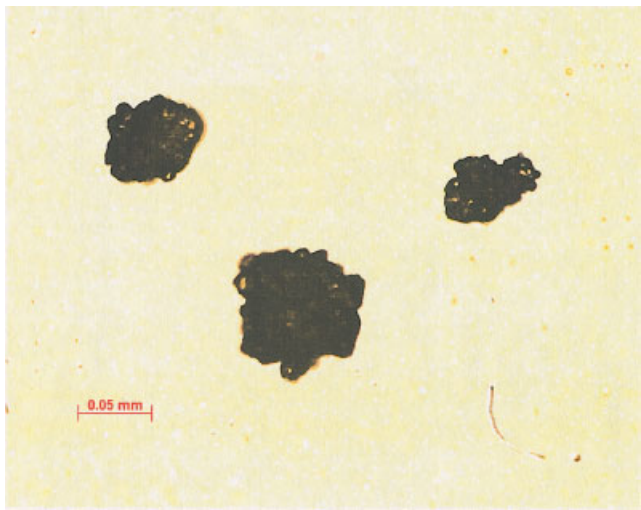


**Figure 5. Photomicrograph for base case in Example 1.**

[Color figure can be viewed in the online issue, which is available at www.interscience.wiley.com]

**Table 6. Results for Example 1**

| | Base Case (Run 1) | Run 2 | Run 3 | Run 4 |
|---|---|---|---|---|
| Formulation and operating conditions | | | | |
| Binder volume, $V$ ($cm^3$) | 394 | 394 | 394 | 500 |
| Binder concentration (wt %) | 5% | 10% | 8% | 8% |
| Binder viscosity, $\mu$ (mPa · s) | 5 | 20 | 14 | 14 |
| Binder flow rate, $\dot{V}$ (g/min) | 11 | 11 | 13 | 13 |
| Results | | | | |
| Mean granule size ($\mu$m) | 50 | 79 | 68 | 79 |
| $CV$ | 0.73 | 1.03 | 0.84 | 0.83 |

m, respectively. Given that $\bar{S}_{\mu}^{a^{cr}} > \bar{S}_{\dot{V}}^{a^{cr}} > \bar{S}_{V}^{a^{cr}}$, binder viscosity was likely to be the most effective parameter in changing the mean granule size. To obtain a desired change of 15 $\mu$m in mean granule size $\Delta a^{cr}$, the required change in viscosity $\Delta\mu$ was estimated from

$$\Delta a^{cr} = \bar{S}_{\mu}^{a^{cr}} \frac{\Delta\mu}{\Delta\mu_{\max}} \tag{30}$$

This gave $\Delta\mu = 15.1$ mPa·s. Therefore, binder viscosity was increased in Run 2 from 5 to 20.1 mPa·s by increasing binder concentration to 10 wt %, following a correlation provided by the vendor (Figure 6). This produced granules with a mean diameter of 79 $\mu$m, but this also led to a wider PSD (CV = 1.03).

Because the CV obtained by increasing binder viscosity from base case to Run 2 overshot the target, the PSD had to be narrowed down by lowering either binder viscosity or flow rate (Table 2). The normalized sensitivity coefficients for parameters that are more effective toward PSD, that is, binder viscosity and flow rate, are

$$\bar{S}_{\mu}^{CV} = \left[\frac{\partial CV}{\partial \psi_a}\frac{\partial \psi_a}{\partial \mu} + \frac{\partial CV}{\partial \tau_p}\frac{\partial \tau_p}{\partial \mu}\right]_{\mu_0} \Delta\mu_{\max} = 1.35\frac{\partial CV}{\partial \tau_p}\frac{V_d^{2/3}}{t_c\varepsilon_b^2 R_{pore}\sigma\cos\theta}\Delta\mu_{\max} \tag{31}$$

$$\bar{S}_{\dot{V}}^{CV} = \left[\frac{\partial CV}{\partial \psi_a}\frac{\partial \psi_a}{\partial \dot{V}} + \frac{\partial CV}{\partial \tau_p}\frac{\partial \tau_p}{\partial \dot{V}}\right]_{\dot{V}_0} \Delta\dot{V}_{\max} = 1.5\frac{\partial CV}{\partial \psi_a}\frac{\Delta\dot{V}_{\max}}{\dot{A}d_d} \tag{32}$$

Using input values in Table 5, $\bar{S}_{\mu}^{CV}$ and $\bar{S}_{\dot{V}}^{CV}$ were calculated to be 0.61 and 0.42, respectively. Because $\bar{S}_{\mu}^{CV} > \bar{S}_{\dot{V}}^{CV}$, binder viscosity was more effective in modifying PSD. However, lowering the viscosity definitely led to a smaller mean size than the desired value. This could be compensated by increasing the binder flow rate. The required changes in binder viscosity and flow rate were then estimated by simultaneously solving the following equations:

$$\Delta a^{cr} = \bar{S}_{\mu}^{a^{cr}} \frac{\Delta\mu}{\Delta\mu_{\max}} + \bar{S}_{V}^{a^{cr}} \frac{\Delta\dot{V}}{\Delta\dot{V}_{\max}} \tag{33}$$

$$\Delta CV = \bar{S}_{\mu}^{CV} \frac{\Delta\mu}{\Delta\mu_{\max}} + \bar{S}_{V}^{CV} \frac{\Delta\dot{V}}{\Delta\dot{V}_{\max}} \tag{34}$$

By specifying $\Delta a^{cr} = 0.5$ $\mu$m and $\Delta CV = -0.18$, and using input values in Table 5, $\Delta\mu$ and $\Delta\dot{V}$ were found to be $-5.72$ mPa·s and $3.82 \times 10^{-8}$ $m^3$ $s^{-1}$, respectively. Therefore, binder viscosity was decreased to 14.3 mPa·s (corresponding to a binder concentration of about 8 wt %) and binder flow rate was increased to 13 g/min in Run 3. This gave granules with a mean diameter of 68 $\mu$m and $CV = 0.84$ (Table 6). Granules were slightly smaller than the desired value albeit with an acceptable size distribution. Because these results were inconsistent with the predictions using Eqs. 33 and 34, $f_1$ and $\partial \mathrm{St}_{def}^*/\partial\mu$ were reestimated to be 0.6 and 12.5 $(\mathrm{Pa{\cdot}s})^{-1}$, respectively, so as to match the experimental results. These updated values were used in subsequent calculations. Note that such reestimation is warranted by the fact that accurate determination of parameters such as $f_1$ and $\mathrm{St}_{def}^*$ is not possible because of the complexity of the related physical phenomena. In the rare case that a reestimated parameter carries an opposite sign compared to that of the original estimation, the user should verify the validity of the assumptions and relationships used in the analysis. More experiments may be needed to provide additional data for making the subsequent move.

The next step was to further increase the mean granule size, without affecting the CV of the PSD. From Table 2, binder volume is the only parameter that is effective on granule size, but not the spread of the PSD. The required change in binder volume could be calculated from

$$\Delta a^{cr} = \bar{S}_{V}^{a^{cr}} \frac{\Delta V}{\Delta V_{\max}} \tag{35}$$

From this equation, a $\Delta V$ of $1.06 \times 10^{-4}$ $m^3$ corresponding to a binder volume of about 500 $cm^3$ was used in the next run. Run 4 produced granules with a mean diameter of 79 $\mu$m and $CV$ of 0.83, which met the target for desirable product attributes.

### *Example 2*

Starch and lactose with hydroxypropyl cellulose as binder are again studied in this example using the Hosokawa Micron Agglomaster™. This example aims at producing granules with a mean diameter between 65 and 70 $\mu$m and porosity between 0.01 and 0.015. Preliminary operating conditions are shown in Table 7. Results of all runs are summarized in Table 8. The

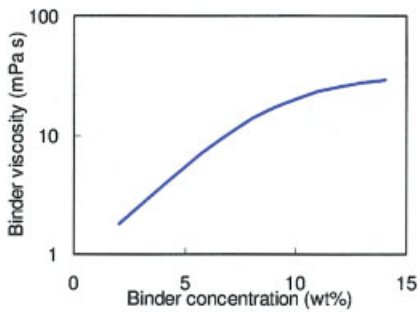


**Figure 6. Correlation between binder viscosity and binder concentration.**

[Color figure can be viewed in the online issue, which is available at www.interscience.wiley.com]

**Table 7. Operating Conditions and Physical Parameters for Example 2**

| | |
|---|---|
| Formulation and operating conditions | |
| Mass of lactose | 350 g |
| Mass of starch | 150 g |
| Binder volume, $V$ | 490 $cm^3$ |
| Binder concentration | 10 wt % |
| Binder viscosity, $\mu$ | 20 mPa · s |
| Binder flow rate, $\dot{V}$ | 15 g/min |
| Binder surface tension, $\sigma$ | 46 mN/m |
| Binder contact angle, $\theta$ | 34° |
| Pure liquid binder density | 1.24 g/mL |
| Fluidized air velocity, $U$ | 0.77 m/s |
| Fluidized air temperature | 50°C |
| Binder spray position | Tangential spray |
| Rotating disc speed | 300 rpm |
| Pulse jet | Off |
| Post-binder-addition time | 15 min |
| Estimated parameters | |
| $h/h_a$ | 8 |
| Surface asperities, $h_a$ | 0.5 $\mu$m |
| Particle density, $\rho_p$ | 2000 $kg/m^3$ |
| Average shear rate inside granulator, $\dot{\gamma}$ | 9000 $s^{-1}$ |
| Coefficient of restitution, $e$ | 0.5 |
| Yield strength, $\tau_y$ | 3000 Pa |
| Critical value for Stokes' number for deformation, $St^*_{def}$ | 0.5 |
| $f_1$ | 0.1 |
| Maximum change of viscosity $\Delta\mu_{max}$ | 15 mPa · s |
| Maximum change of binder flow rate $\Delta\dot{V}_{max}$ | $2 \times 10^{-7}$ $m^3/s$ |
| Maximum change of binder volume $\Delta V_{max}$ | $2 \times 10^{-4}$ $m^3$ |
| Maximum change of fluidized air velocity $\Delta U_{max}$ | 1.2 m/s |
| $\frac{\partial h}{\partial \dot{V}}$ | 10 $s/m^2$ |
| $\frac{\partial h}{\partial V}$ | 0.001 $m^{-2}$ |
| $\frac{\partial h}{\partial U}$ | $-1 \times 10^{-6}$ s |
| $\frac{\partial St^*_{def}}{\partial \mu}$ | 5 $(Pa \cdot s)^{-1}$ |
| $\frac{\partial St^*_{def}}{\partial \dot{V}}$ | $6 \times 10^5$ $s/m^3$ |
| $\frac{\partial St^*_{def}}{\partial V}$ | 100 $m^{-3}$ |
| $\frac{\partial St^*_{def}}{\partial U}$ | −0.1 s/m |

base case produced granules with a mean diameter of 50 $\mu$m and porosity of 0.021, as measured by a laser diffraction particle size analyzer (Model LS13320, Beckman Coulter) and BET gas adsorption (Model Autosorb-1 and Ultrapycnometer 1000, Quantachrome Instruments), respectively.

Because the granules produced in the trial run did not meet the specifications, improvements were attempted using the qualitative and quantitative analyses described in the procedure. The dominant force inside granules was identified using input values from Table 7. A capillary number of 0.34 indicates that the viscous effect dominates. From Table 2, binder viscosity, binder volume, and process intensity are identified to have an effect on both mean granule size and porosity, whereas binder flow rate affects only the mean granule size. Process intensity can be represented by the fluidized air flow rate in this example.

Next, sensitivity analysis on granule porosity and size was carried out with respect to these parameters. According to Table 3, granule porosity can be expressed as

$$\varepsilon = \varepsilon(\mu, V, U, h) \tag{36}$$

Because the viscous effect is dominant, Eqs. 22–24 were used to obtain normalized sensitivity coefficients for granule porosity. Using input values from Table 7, $\bar{S}^{\varepsilon}_{U}$, $\bar{S}^{\varepsilon}_{\mu}$, and $\bar{S}^{\varepsilon}_{V}$ were calculated to be −0.096, 0.047, and 0.02, respectively. Because the absolute value of $\bar{S}^{\varepsilon}_{U}$ is the largest, fluidized air flow rate was expected to have the greatest effect on granule porosity.

Sensitivity analysis was also carried out on granule size using Eqs. 27–29. The calculated values were $3.08 \times 10^{-5}$, $1.12 \times 10^{-5}$, and $1.23 \times 10^{-6}$ m for $\bar{S}^{a^{cr}}_{\mu}$, $\bar{S}^{a^{cr}}_{\dot{V}}$, and $\bar{S}^{a^{cr}}_{V}$, respectively. To calculate the normalized sensitivity coefficient of fluidized air flow rate, Eq. 11 is differentiated with respect to $U$ and normalized using Eq. 9. Using input values from Table 7, $\bar{S}^{a^{cr}}_{U} = -7.37 \times 10^{-6}$ m. By comparing the absolute values of the normalized sensitivity coefficients, binder viscosity was found to have the greatest effect on granule size. An option was to simultaneously change fluidized air flow rate and binder viscosity. The required changes can be estimated by solving

$$\Delta\varepsilon = \bar{S}^{\varepsilon}_{U}\frac{\Delta U}{\Delta U_{max}} + \bar{S}^{\varepsilon}_{\mu}\frac{\Delta\mu}{\Delta\mu_{max}} \tag{37}$$

$$\Delta a^{cr} = \bar{S}^{a^{cr}}_{U}\frac{\Delta U}{\Delta U_{max}} + \bar{S}^{a^{cr}}_{\mu}\frac{\Delta\mu}{\Delta\mu_{max}} \tag{38}$$

By specifying $\Delta\varepsilon = -0.0085$ and $\Delta a^{cr} = 8.75$ $\mu$m, $\Delta U$ and $\Delta\mu$ were determined to be 0.28 m/s and 5.5 mPa·s, respectively. This gave a fluidized air flow rate of 1.05 m/s and binder viscosity of 25.5 mPa·s (binder concentration = 12 wt %). Experiments with modified operating conditions produced granules with a diameter of 58 $\mu$m and a porosity of 0.011. Because experimental results were different from estimations in sensitivity analysis, the values of $\partial h/\partial U$ and $\partial St^*_{def}/\partial\mu$ were

**Table 8. Results for Example 2**

| | Base Case | Run 2 | Run 3 |
|---|---|---|---|
| Formulation and operating conditions | | | |
| Fluidized air velocity, $U$ (m/s) | 0.77 | 1.05 | 1.05 |
| Binder concentration (wt %) | 10% | 12% | 12% |
| Binder viscosity, $\mu$ (mPa · s) | 20 | 25.5 | 25.5 |
| Binder flow rate, $\dot{V}$ (g/min) | 15 | 15 | 20 |
| Results | | | |
| Mean granule size ($\mu$m) | 50 | 58 | 68 |
| Granule porosity | 0.021 | 0.011 | 0.013 |

**Table 9. Operating Conditions for Example 3**

| | |
|---|---|
| Formulation and operating conditions for base case | |
| Mass of lactose | 315 g |
| Mass of starch | 125 g |
| Mass of paracetamol | 50 g |
| Binder volume, $V$ | 391 $cm^3$ |
| Binder concentration | 5 wt % |
| Binder spray position | Tangential spray |
| Binder flow rate, $\dot{V}$ | 15 g/min |
| Fluidized air temperature | 60°C |
| Fluidized air velocity, $U$ | 0.8 m/s |
| Rotating disc speed | 300 rpm |
| Pulse jet | Off |

reestimated to be $-3.5 \times 10^{-6}$ s and 4 $(Pa{\cdot}s)^{-1}$, respectively, to match the experimental results.

Although the granule porosity was within the desired range, the mean granule size was too small. Given that qualitative analysis shows that binder flow rate is the only parameter that is effective in modifying mean granule size but does not affect porosity, Run 3 was performed with a higher binder flow rate. The necessary increase in binder flow rate was estimated from

$$\Delta a^{cr} = \bar{S}_V^{a^{cr}} \frac{\Delta \dot{V}}{\Delta \dot{V}_{\max}} \tag{39}$$

The estimated $\Delta \dot{V}$ from this equation was $8.1 \times 10^{-8}$ $m^3/s$, which corresponded to a binder flow rate of about 20 g/min. Performing the experiment using the modified operating conditions gave granules with a mean diameter of 68 $\mu$m and a porosity of 0.013, values that were both within the specifications.

### *Example 3*

The uniformity of the spatial distribution of paracetamol within and among granules containing starch and lactose with hydroxypropyl cellulose as binder is studied. Paracetamol represents an active pharmaceutical ingredient present at a mass fraction of about 0.1. Time-of-flight secondary ion mass spectrometry (ToF-SIMS; Model PHI 7200, Physical Electronics) was used to characterize the content uniformity. In ToF-SIMS, a pulsed primary ion beam strikes the sample surface so that secondary ions are extracted from the sample. A histogram of counts at different mass to charge ($m/z$) ratio is obtained and, at a defined $m/z$ ratio, a map of counts over the sample surface is also available. A more detailed review of this technique can be found in Chan and Weng.[35]

After performing ToF-SIMS analysis of pure components, the representative peak for paracetamol was found at an $m/z$ ratio of 152. Therefore, the analysis focused on maps at this $m/z$ ratio. The counts (level of whiteness) represent the strength of the signal (secondary ions) from the granule surface. The counts on a map were summed up along the $y$-axis and the mean and standard deviation among these sums at different $x$-axis values were calculated. A lower ratio of standard deviation to mean represents a more uniform distribution. Operating at base case conditions (Table 9)—a binder flow rate of 15 g/min and a binder concentration of 5 wt %—showed a relatively nonuniform distribution of paracetamol among granules (Figure 7a, standard deviation/mean = 0.74 $count^{-1}$). To ob-

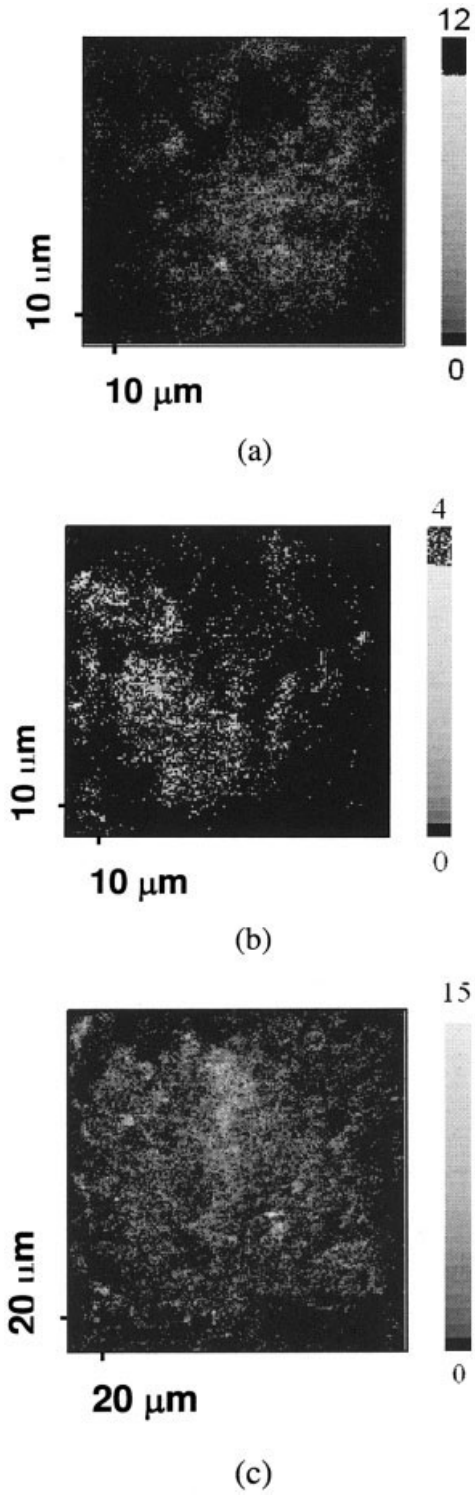


**Figure 7. ToF-SIMS results for Example 3.**

(a) Binder flow rate = 15 g/min, mean = 0.325 count, standard deviation (SD) = 0.241, SD/mean = 0.74 $(count)^{-1}$; (b) binder concentration = 2.5 wt %, mean = 0.159 count, SD = 0.128, SD/mean = 0.81 $(count)^{-1}$; (c) binder flow rate = 10 g/min, mean = 0.7 $(count)^{-1}$, SD = 0.431, SD/mean = 0.62 $(count)^{-1}$.

tain granules with better content uniformity, either binder flow rate or binder viscosity (binder concentration) should be reduced (Table 2). The results of the corresponding trials are shown in Figures 7b and 7c, respectively. The results show that lowering binder viscosity did not give the expected trend, which may be explained by the fact that understanding of the effect of operating variables on content uniformity of granules is still in a preliminary stage. Decreasing the binder flow rate to 10 g/min did give a more uniform distribution of paracetamol among granules (standard deviation/mean = 0.62 count$^{-1}$), which agrees with the expectation from Table 2.

## Conclusions

Granulation is widely used in a number of industries. Despite significant advances in understanding its phenomena, it is still very challenging to obtain, in a systematic manner, granules with the desired attributes. This article presents a novel approach in integrating analyses with experiments to determine the operating conditions of a granulator that would produce granules with the desired attributes. Starting with the results of a base case experiment, necessary modifications to the formulation and operating conditions are identified for a subsequent experiment. All candidate parameters are qualitatively screened to identify the most effective ones; sensitivity analyses are then performed to quantify the effects. This analysis–experiment cycle is repeated until granules with the desired product attributes are obtained.

The iterative procedure allows effective use of available models despite the fact that values of some model parameters are not known. A rough estimate of these parameters is often sufficient for the model to reveal the correct trend. As more data become available, these estimates are updated in subsequent runs to improve the accuracy in the prediction of the operating parameters. In contrast to factorial design, which simultaneously investigates the effects of multiple factors,[36,37] the operating parameters in each run are determined based on the results of previous runs. Given the numerous variables affecting the product attributes, such an approach minimizes the number of runs required to determine the desirable operating conditions, when compared to the factorial design. This definitely speeds up the development of a granulation process.

The procedure can be expanded to involve additional operating parameters, models, and product attributes to allow for wider applicability. A severe limitation is the availability of suitable models arising from the complexity of the phenomena involved in granulation. The assumptions used in deriving a model often limit its validity within a certain range of conditions. For example, models discussed in the procedure are developed for continuous mode or under equilibrium conditions. Therefore, they do not fully describe the transient behavior of a batch granulation process, for which a model with more parameters would be necessary. Indeed, there is always a compromise between model accuracy and uncertainties in model parameters. Experimental techniques or simulation tools for estimating these parameters such as neural network and discrete element models would be valuable additions to this procedure. Efforts in these directions are under way.


## Acknowledgments

The financial support of Research Grants Council (HKUST 602703) for this work is gratefully acknowledged.


## Notation

$a$ = granule radius, m
$\dot{A}$ = powder flux through spray zone, m$^2$/s
$C$ = material constant in Eq. 25
$Ca$ = capillary number, dimensionless
$CV$ = coefficient of variation, dimensionless
$d_d$ = binder droplet diameter, m
$d_{16}$, $d_{50}$, $d_{84}$ = particle size corresponding to 16, 50, and 84% weight fraction on the cumulative PSD, m
$e$ = coefficient of restitution, dimensionless
$f_1$ = coefficient in Eq. 11 representing the importance of layering on granule growth, dimensionless
$f(\mu)$ = function of coefficient of sliding friction at interparticle contacts, dimensionless
$F_{c0}$ = constant signifying the capillary force at zero porosity, dimensionless
$g$ = gravitational acceleration constant, m/s$^2$
$h$ = thickness of binder liquid layer, m
$h_a$ = characteristic length scale of the surface asperities, m
$H_{\max}$ = maximum height of granule fall in granulator, m
$K_\varepsilon$ = dimensionless granule compaction rate, dimensionless
$n$ = correlation coefficient in Eq. 7, dimensionless
$N$ = number of particles inside a granule, dimensionless
$P$ = product attribute
$\mathbf{q}$ = vector including all the intermediate variables in granulation
$R_{pore}$ = pore radius, m
$s$ = liquid pore saturation in Eq. 25 and Figure 1, dimensionless
$S$ = sensitivity coefficient
$\bar{S}$ = normalized sensitivity coefficient
St = Stokes' number, dimensionless
$t_c$ = circulation time, s
$t_p$ = drop penetration time, s
$U$ = relative velocity between particles, m/s
$V$ = binder volume, m$^3$
$\dot{V}$ = binder volumetric spray rate, m$^3$/s
$V_d$ = binder drop volume, m$^3$
$V_e$ = volume of void space excluding binder layer inside granules, m$^3$
$V_p$ = volume of particle, m$^3$
$V_v$ = volume of void space, m$^3$
$w$ = mass ratio of liquid to solid, dimensionless
$\Delta x$ = reduction in interparticle gap distance, m

### *Greek letters*

$\boldsymbol{\alpha}$ = vector of equipment parameters in granulation
$\Delta\alpha_{j,\max}$ = maximum expected range of $\alpha_j$
$\boldsymbol{\beta}$ = vector of nonequipment parameters in granulation
$\varepsilon$ = granule porosity, dimensionless
$\varepsilon_b$ = powder bed porosity, dimensionless
$\phi(s)$ = function of granule saturation and particle assembly, dimensionless
$\dot{\gamma}$ = average shear rate inside granulator, s$^{-1}$
$\lambda_{LS}$ = spreading coefficient of liquid over solid, N/m
$\mu$ = viscosity, kg m$^{-1}$ s$^{-11}$
$\theta$ = contact angle, rad
$\rho_l$ = liquid binder density, kg/m$^3$
$\rho_p$ = particle density, kg/m$^3$
$\rho_s$ = solid powder density, kg/m$^3$
$\sigma$ = binder surface tension, N/m
$\sigma_t$ = granule tensile strength, Pa
$\tau_p$ = dimensionless penetration time, dimensionless
$\tau_y$ = yield strength, Pa
$\psi_a$ = dimensionless spray flux, dimensionless

### *Subscripts*

$i, j, k$ = indices
$c$ = capillary effect
$coal$ = coalescence
$def$ = deformation
max = maximum
min = minimum
$v$ = viscous effect
0 = initial value
1 = represents parameters before consolidation
2 = represents parameters after consolidation

### *Superscript*

*, $cr$ = critical value

## Literature Cited


1. Ennis BJ. Unto dust shalt thou return. In Behringer RP, Jenkins JT, eds. *Powders and Grains.* Rotterdam, The Netherlands: Balkema; 1997:13.
2. Baum RM. Outlook for pharmaceuticals. *Chem Eng News.* 2004;82:3.
3. Iveson SM, Litster JD, Hapgood K, Ennis BJ. Nucleation, growth and breakage phenomena in agitated wet granulation processes: A review. *Powder Technol.* 2001a;117:3-39.
4. Ennis BJ, Li J, Tardos GI, Pfeffer R. The influence of viscosity on the strength of an axially strained pendular liquid bridge. *Chem Eng Sci.* 1990;45:3071-3088.
5. Litster JD, Hapgood KP, Michaels JN, Sims A, Roberts M, Kameni SK, Hsu T. Liquid distribution in wet granulation: Dimensionless spray flux. *Powder Technol.* 2001;114:32-39.
6. Hapgood KP, Litster JD, Smith R. Nucleation regime map for liquid bound granules. *AIChE J.* 2003;49:350-361.
7. Iveson SM, Litster JD, Ennis BJ. Fundamental studies of granule consolidation: Part 1. Effects of binder content and binder viscosity. *Powder Technol.* 1996;88:15-20.
8. Iveson SM, Litster JD. Fundamental studies of granule consolidation: Part 2. Quantifying the effects of particle and binder properties. *Powder Technol.* 1998;99:243-250.
9. Iveson SM, Wauters PAL, Forrest S, Litster JD, Meesters GMH, Scarlett B. Growth regime map for liquid-bound granules: Further development and experimental validation. *Powder Technol.* 2001b; 117:83-97.
10. Ouchiyama N, Tanaka T. Stochastic model for compaction of pellets in granulation. *Ind Eng Chem Fundam.* 1980;19:555-560.
11. Ennis BJ, Tardos GI, Pfeffer R. A microlevel-based characterization of granulation phenomena. *Powder Technol.* 1991;65:257-272.
12. Ouchiyama N, Tanaka T. The probability of coalescence in granulation kinetics. *I&EC Process Des Dev.* 1975;14:286-289.
13. Liu LX, Litster JD, Iveson SM, Ennis BJ. Coalescence of deformable granules in wet granulation processes. *AIChE J.* 2000;46:529-539.
14. Heinrich S, Peglow M, Morl L. Unsteady and steady-state particle size distributions in batch and continuous fluidized bed granulation systems. *Chem Eng J.* 2002;86:223-231.
15. Cryer SA. Modeling agglomeration processes in fluid-bed granulation. *AIChE J.* 1999;45:2069-2078.
16. Heinrich S, Morl L. Fluidized bed spray granulation—A new model for the description of particle wetting and of temperature and concentration distribution. *Chem Eng Process.* 1999;38:635-663.
17. Heinrich S, Blumschein J, Henneberg M, Ihlow M, Peglow M, Morl L. Study of dynamic multi-dimensional temperature and concentration distributions in liquid-sprayed fluidized beds. *Chem Eng Sci.* 2003;58: 5135-5160.
18. Cryer SA, Scherer PN. Observations and process parameter sensitivities in fluid-bed granulation. *AIChE J.* 2003;49:2802-2809.
19. Parikh DM, ed. *Handbook of Pharmaceutical Granulation Technology.* New York, NY: Marcel Dekker; 1997.
20. Fung KY, Ng KM. Product-centered processing: Pharmaceutical tablets and capsules. *AIChE J.* 2003;49:1193-1215.
21. Wibowo C, Ng KM. Synthesis of bulk solids processing systems. *AIChE J.* 1999;45:1629-1648.
22. Sommer K. Size enlargement. In *Ullmann's Encyclopedia of Industrial Chemistry, Vol. B2*. Fifth Edition. Weinheim, Germany: VCH; 1988.
23. Snow RH, Allen T, Ennis BJ, Litster JD. Size reduction and size enlargement. In Perry RH, Green DW, Maloney JO, eds. *Perry's Chemical Engineers' Handbook.* Seventh Edition. New York, NY: McGraw-Hill; 1997.
24. Pietsch W. *Agglomeration Processes: Phenomena, Technologies, Equipment.* Weinheim, Germany: VCH; 2002.
25. Kibbe AH, ed. *Handbook of Pharmaceutical Excipients*. Third Edition. Washington, DC: American Pharmaceutical Association; 2000.
26. Khankari RK, Hontz J. Binders and solvents. In Parikh DM, ed. *Handbook of Pharmaceutical Granulation Technology.* New York, NY: Marcel Dekker; 1997:59-74.
27. Iveson SM, Beathe JA, Page NW. The dynamic strength of partially saturated powder compacts: The effect of liquid properties. *Powder Technol.* 2002;127:149-161.
28. Rowe RC. Binder-substrate interactions in granulation: A theoretical approach based on surface free energy and polarity. *Int J Pharm.* 1989;52:149-154.
29. Ennis BJ. Agglomeration and size enlargement session summary paper. *Powder Technol.* 1996;88:203-225.
30. Mort PR, Tardos GI. Scale-up of agglomeration processes using transformations. *Kona.* 1999;17:64-75.
31. Kelkar VV, Ng KM. Screening procedure for synthesizing isothermal multiphase reactors. *AIChE J.* 1998;44:1563-1578.
32. Tardos GI, Khan MI, Mort PR. Critical parameters and limiting conditions in binder granulation of fine powders. *Powder Technol.* 1997;94:245-258.
33. Hapgood KP, Litster JD, Biggs SR, Howes T. Drop penetration into porous powder beds. *J Colloid Interface Sci.* 2002;253:353-366.
34. Rumpf H. The strength of granules and agglomerates. In Knepper WA, ed. *Agglomeration.* New York, NY: Interscience; 1962.
35. Chan CM, Weng LT. Applications of X-ray photoelectron spectroscopy and static secondary ion mass spectrometry in surface characterization of copolymers and polymer blends. *Rev Chem Eng.* 2000;16: 341-408.
36. Merkku P, Yliruusi J. Use of 3(3) factorial design and multilinear stepwise regression-analysis in studying the fluidized-bed granulation process. Part I. *Eur J Pharm Biopharm*. 1993a;39:75-81.
37. Merkku P, Antikainen O, Yliruusi J. Use of 3(3) factorial design and multilinear stepwise regression-analysis in studying the fluidized-bed granulation process. Part II. *Eur J Pharm Biopharm.* 1993b;39:112-116.


## Appendix: Derivation of Eq. 24

Collision in a wet granulation process is modeled as two equal-size spheres with wet surfaces approaching each other. As the two spheres draw closer together, the two liquid layers merge and the combined liquid layer is squeezed out. In a similar way, consolidation under dominant viscous effect is modeled as equal-size spheres with wet surfaces getting closer to each other such that the granule porosity becomes smaller.

Figure A1a shows the initial condition before consolidation, in which particles with radius $a$ are separated at a distance of $2h_1$ from each other. The total volume of particles in a granule ($V_p$) can be expressed as

$$V_p = \frac{4\pi a^3 N}{3} \tag{A1}$$

where $N$ is the number of particles inside granules. By drawing a control volume in the shape of a sphere with radius $a + h_1$ around each particle, the void volume in a granule (after the liquid binder is removed) before consolidation ($V_{v,1}$) can be expressed as

$$V_{v,1} = \frac{4\pi}{3}[(a + h_1)^3 - a^3]N + V_{e,1} \tag{A2}$$

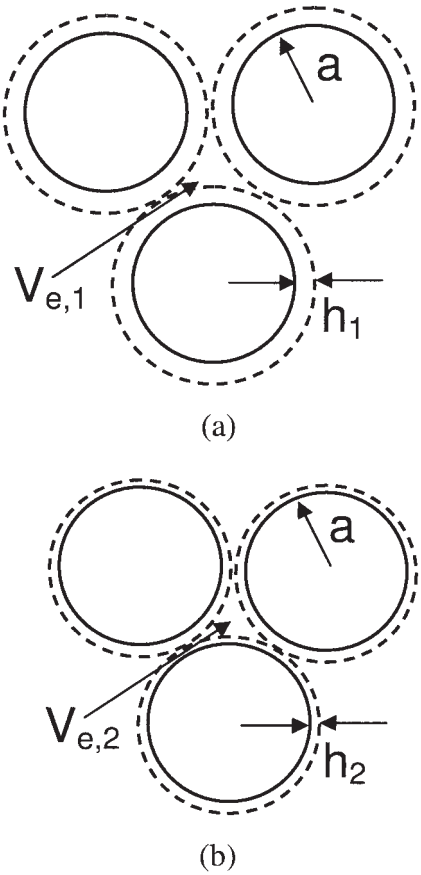


**Figure A1. Granules before consolidation (a) and after consolidation (b).**

where $V_{e,1}$ represents the amount of void volume outside of the control volume. From the definition of granule porosity,

$$\varepsilon_1 = \frac{V_{v,1}}{V_p + V_{v,1}} = 1 - \frac{\frac{4\pi}{3}a^3}{\frac{4\pi}{3}(a + h_1)^3 + \frac{V_{e,1}}{N}} \tag{A3}$$

By rearranging this equation, an expression for $V_{e,1}/N$ in terms of $\varepsilon_1$ can be developed:

$$\frac{V_{e,1}}{N} = \frac{4\pi[a^3 - (a + h_1)^3(1 - \varepsilon_1)]}{3(1 - \varepsilon_1)} \tag{A4}$$

Similarly, the final condition after consolidation is shown by Figure A1b, in which the particles are now separated at a distance of $2h_2$ from each other. By choosing a sphere with radius $a + h_2$ around each particle as the control volume, and assuming that the particles stay intact during consolidation, expressions similar to Eqs. A2 and A3 can be developed for the void volume and granule porosity after consolidation. Note that the control volume can be viewed as a collection of randomly packed equal-size spheres, with a smaller radius after consolidation. Assuming there is no significant rearrangement of the spheres, the void fraction in such a system is constant regardless of the radius of the spheres. In other words, $V_e/(V_v + V_p)$ stays constant during consolidation, or

$$\frac{\frac{V_{e,1}}{N}}{\frac{4\pi}{3}(a + h_1)^3 + \frac{V_{e,1}}{N}} = \frac{\frac{V_{e,2}}{N}}{\frac{4\pi}{3}(a + h_2)^3 + \frac{V_{e,2}}{N}} \tag{A5}$$

which implies that

$$\frac{\frac{4\pi}{3}(a + h_1)^3}{\frac{4\pi}{3}(a + h_1)^3 + \frac{V_{e,1}}{N}} = \frac{\frac{4\pi}{3}(a + h_2)^3}{\frac{4\pi}{3}(a + h_2)^3 + \frac{V_{e,2}}{N}} \tag{A6}$$

The change of porosity during consolidation ($\Delta\varepsilon$) is

$$\Delta\varepsilon = \varepsilon_2 - \varepsilon_1 = \frac{\frac{4\pi}{3}a^3}{\frac{4\pi}{3}(a + h_1)^3 + \frac{V_{e,1}}{N}} - \frac{\frac{4\pi}{3}a^3}{\frac{4\pi}{3}(a + h_2)^3 + \frac{V_{e,2}}{N}} \tag{A7}$$

Substituting Eq. A6 gives

$$\Delta\varepsilon = \frac{\frac{4\pi}{3}a^3}{\frac{4\pi}{3}(a + h_1)^3 + \frac{V_{e,1}}{N}}\left[1 - \frac{(a + h_1)^3}{(a + h_2)^3}\right]$$

After substituting Eq. A4 and simplifying, we get

$$\Delta\varepsilon = (1 - \varepsilon_1)\left[1 - \left(\frac{a + h_1}{a + h_2}\right)^3\right] \tag{A8}$$

By replacing $h_2$ by $h_1 + \Delta h$ and taking the limit as $\Delta h$ approaches zero, we obtain

$$\lim_{\Delta h \to 0}\frac{\Delta\varepsilon}{\Delta h} = \left.\frac{d\varepsilon}{dh}\right|_{\varepsilon_1, h_1} = \frac{3(1 - \varepsilon_1)}{a + h_1} \tag{A9}$$

*Manuscript received Nov. 9, 2005, and revision received Jun. 3, 2006.*